Journal of Power Sources 195 (2010) 1435–1440

Contents lists available at ScienceDirect

Journal of Power Sources

journal homepage: www.elsevier.com/locate/jpowsour

Short communication

Design for segmented-in-series solid oxide fuel cell through mathematical modeling

Daan Cui [a,b,c], Mojie Cheng [a,b,*]

[a] Dalian National Laboratory for Clean Energy, Dalian 116023, China
[b] Dalian Institute of Chemical Physics, Chinese Academy of Sciences, Dalian 116023, China
[c] Graduate School of the Chinese Academy of Sciences, Beijing 100049, China

ARTICLE INFO

Article history:
Received 21 July 2009
Received in revised form 9 September 2009
Accepted 9 September 2009
Available online 16 September 2009

Keywords:
Solid oxide fuel cell
Segmented-in-series
Modeling
Optimization

ABSTRACT

The segmented-in-series solid oxide fuel cell comprising fuel channel, anode, cathode and electrolyte layers has been evaluated by developing a two-dimensional model, in which the equations have been solved numerically through finite element methods. The results indicate that the voltage of each membrane electrode assembly (MEA) exhibits a parabola-like curve and is higher than the appointed voltage of unit cell (0.7 V). From fuel inlet to outlet, the voltage of each MEA deceases due to the decreasing local H_2 concentration. When both the interconnector and electrolyte gap lengths are fixed, the cell module with 5 mm long anode gives the maximal power density for the SS-SOFC. Higher power densities can be achieved through increasing the cathode thickness.

1. Introduction

Solid oxide fuel cell (SOFC) is one of the most promising candidates for power generation because of its high efficiency, clean generation of electric power and silent work [1–3]. The segmented-in-series SOFC (SS-SOFC) has a short current path compared with tubular SOFC and the less need for gas-tight seals relative to planar SOFC [4–6]. Recently, SS-SOFC has been implemented in a circular tubular and a flat tubular configuration. Several different schematics of SS-SOFC were proposed in different literatures [4–10]. A fundamental principle ought to be clarified to avoid the short circuit current inside the cell. Such as, the short circuit current can occur from the design of Fig. 1 [4] because oxygen anion can flow through two paths according to the directions of two arrows shown in Fig. 1.

As ohmic losses account for a large part of the overall losses, the previous investigations [4–6] mainly focus on ohmic losses in SS-SOFC. Besides the estimation of the influence of ohmic resistance on cell performance, some other phenomena should also be analyzed in detail for a better understanding of this type of cells. For examples, the effects of both ohmic losses and fuel concentration distribution on the voltage of unit cell in the SS-SOFC. An extensive model including activation and concentration effects should also be given for cell geometrical optimization through finite element methods (FEM).

In the present work, a tubular SS-SOFC comprising fuel channel, anode, cathode and electrolyte layers will be evaluated by developing a two-dimensional (2D) model. The model covers the electrochemical reaction, electrical and species transport, and the equations in this model can be solved through FEM. The distributions of electrical potential and fuel concentration in the cell will be estimated. The mathematical model will be used to carry out the improvement of the cell geometry.

2. Numerical model

Fig. 2 shows the schematic of SS-SOFC geometry in 2D model. The 2D model is axisymmetric, and the dash-dotted line is the symmetric axis. H_2 humidified at room temperature is introduced as a fuel at a volume flow rate of 30 cm^3 min^{-1}. Oxygen concentration at the cathodic surface is assumed to be the same as in air. The models of cell module of the different dimension are established to investigate the effect of the cell structure on cell performance. Fig. 2 shows a schematic of the repetitive unit of the SS-SOFC as well. It is assumed that interconnector and electrolyte gap lengths are fixed at all the process of calculations. The interconnector and electrolyte gap lengths are 1.5 and 2 mm, respectively. The material properties are listed in Table 1. The SS-SOFC model chooses the electrolyte thickness of 10 μm and the anode thickness of 20 μm. The cathodic thickness and the inner radius of the anode channel are changed. Because of the cathodic conductivity being lower than the anodic conductivity, it is considered to change the cathodic

* Corresponding author at: Dalian Institute of Chemical Physics, Chinese Academy of Sciences, 457 Zhongshan Road, Dalian, Liaoning 116023, China. Tel.: +86 411 84379049; fax: +86 411 84379049.
E-mail address: mjcheng@dicp.ac.cn (M. Cheng).

0378-7753/$ – see front matter © 2009 Elsevier B.V. All rights reserved.
doi:10.1016/j.jpowsour.2009.09.020

Nomenclature

c	concentration (mol m^{-3})
D_{ij}	diffusion coefficient (m^2 s^{-1})
F	Faraday's constant (96,485 C mol^{-1})
i	local current density (A m^{-2})
n_e	electron transferred per reacting
P	pressure (Pa)
R_g	gas constant (8.314 J mol^{-1} K^{-1})
T	temperature (K)
u	velocity (m s^{-1})

Greek letters

β	transfer coefficient
ρ	density (kg m^{-3})
σ	conductivity (S m^{-1})
ϕ	potential (V)

Subscripts and superscripts

a	anode
c	cathode
ele	electrolyte
rev	reversible

thickness rather than the anodic in this paper. The thickness of the support substrate of the SS-SOFC is 1 mm. The total length of cell module is about 40 mm, which depends on both the anode length and number of unit cell. The cell dimensions of the different anode length are shown in Table 2.

In this steady state model, the reactant gas mixtures are approximated as ideal gas. The electrochemical reactions are considered

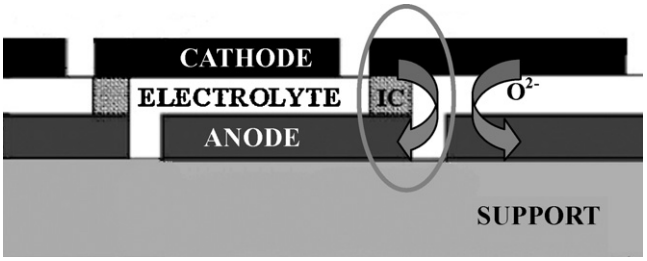

Fig. 1. Schematic drawing of the SS-SOFC geometry in Ref. [4].

Table 1
Input parameters to model [2,3,11].

Descriptions	Symbol	Value
Anode thickness (μm)		20
Electrolyte thickness (μm)		10
Anode conductivity (S m^{-1})	σ_a	$95 \times 10^6\, T^{-1} \exp(-1150/T)$
Cathode conductivity (S m^{-1})	σ_c	$42 \times 106\, T^{-1} \exp(-1200/T)$
Electrolyte conductivity (S m^{-1})	σ_{ele}	$3.34 \times 10^4 \exp(-10{,}300/T)$
Interconnector conductivity (S m^{-1})	σ_{ic}	40
Transfer coefficient	β	0.5
Activation energy of anode (J mol^{-1})	$E_{act,a}$	140,000
Electron transferred per reacting	n_e	1
Hydrogen diffusion coefficient (m^2 s^{-1})	$D_{H_2,a}$	3.14e−5
H_2O diffusion coefficient (m^2 s^{-1})	$D_{H_2O,a}$	1.39e−5
Gas diffusion coefficient in anodic channel (m^2 s^{-1})	D_a	8.506e−4
Oxygen diffusion coefficient (m^2 s^{-1})	$D_{O_2,c}$	7.588e−6

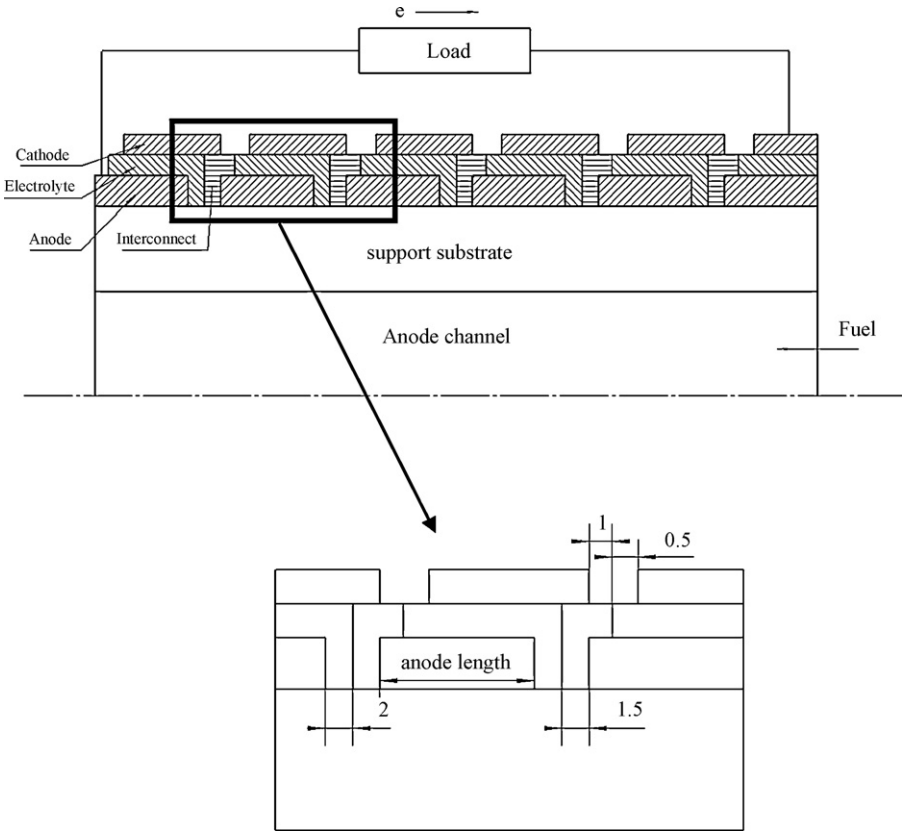

Fig. 2. Schematic drawing and repetitive unit of a section of the SS-SOFC geometry.

Table 2
Cell dimensions of different anode length.

Anode length (mm)	Unit cell length (mm)	Unit cell number	Active length of cell module (mm)	Total length of cell module (mm)
3	1.5	7	10.5	42
4	2.5	6	15	41.5
5	3.5	5	17.5	39
7	5.5	4	22	38.5
10	8.5	3	25.5	37
18	16.5	2	33	40

to take place only at the electrode/electrolyte interface. The model is assumed to be isothermal and the cell module runs at 800 °C. It is assumed that the average voltage of each unit cell is 0.7 V for the operation of SS-SOFC. For example, when there are 7 unit cells, the cell module voltage is $7 \times 0.7 = 4.9$ V. The model makes use of the differential equations which are integrated in the 2D domains through commercial software, COMSOL MULTIPHYSICS®. Input parameters of the model are shown in Table 1.

The Butler–Volmer kinetic equations are generally adopted for expressing the local current density distribution:

$$i_a = i_{a,0}^{H_2} \cdot \frac{(p_{H_2})^{0.25}}{(p_{H_2O})^{0.5}} \exp\left(\frac{-E_{act,a}}{R_g \cdot T}\right) \times \left\{\exp\left(\beta \frac{n_e \cdot F \cdot (\phi_{rev} - |\phi_a - \phi_{ele}|)}{R_g \cdot T}\right) - \exp\left[-(1-\beta)\frac{n_e \cdot F \cdot (\phi_{rev} - |\phi_a - \phi_{ele}|)}{R_g \cdot T}\right]\right\} \quad (1)$$

$$i_c = i_{c,0}^{O_2} \cdot \frac{(p_{O_2}/p_{O_2}^0)^{1/4}}{1 + (p_{O_2}/p_{O_2}^0)^{1/2}} \times \left\{\exp\left(\beta \frac{n_e \cdot F \cdot (\phi_{rev} - |\phi_c - \phi_{ele}|)}{R_g \cdot T}\right) - \exp\left[-(1-\beta)\frac{n_e \cdot F \cdot (\phi_{rev} - |\phi_c - \phi_{ele}|)}{R_g \cdot T}\right]\right\} \quad (2a)$$

$$p_{O_2}^0 \text{ (Pa)} = 4.9 \times 10^3 \exp\left(-\frac{2 \times 10^5}{R_g \cdot T}\right) \quad (2b)$$

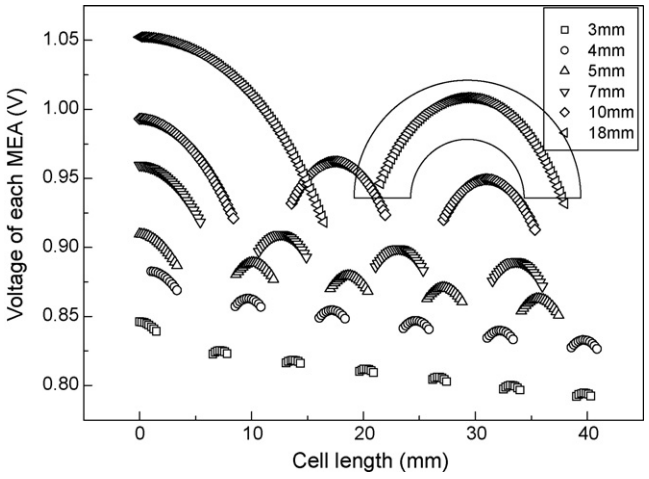

Fig. 4. The voltage (V) of each MEA for the different anode length with the support substrate of 0.8 mm inner radius and the cathode of 50 μm thickness.

In Eqs. (1) and (2a), the anodic exchange current density, $i_{a,0}^{H_2}$ is 3.4×10^{10} A m^{-2} for a Ni-YSZ anode [12]. The cathodic exchange current density, $i_{c,0}^{O_2}$ is 4000 A m^{-2} for a LSM-YSZ cathode [3]. The values of $i_{a,0}^{H_2}$ and $i_{c,0}^{O_2}$ have been used in the FEM model of SOFC [3], where the results showed that the model agrees well with the experimental data. ϕ_{rev} can be obtained from Nernst equation. Electron and ion charge conservation at the electrode and electrolyte is expressed by Eq. (3):

$$-\nabla(\sigma \cdot \nabla\phi) = 0 \quad (3)$$

The steady state diffusion and convection equation, Eq. (4) is solved to obtain the species distribution of reactants and products

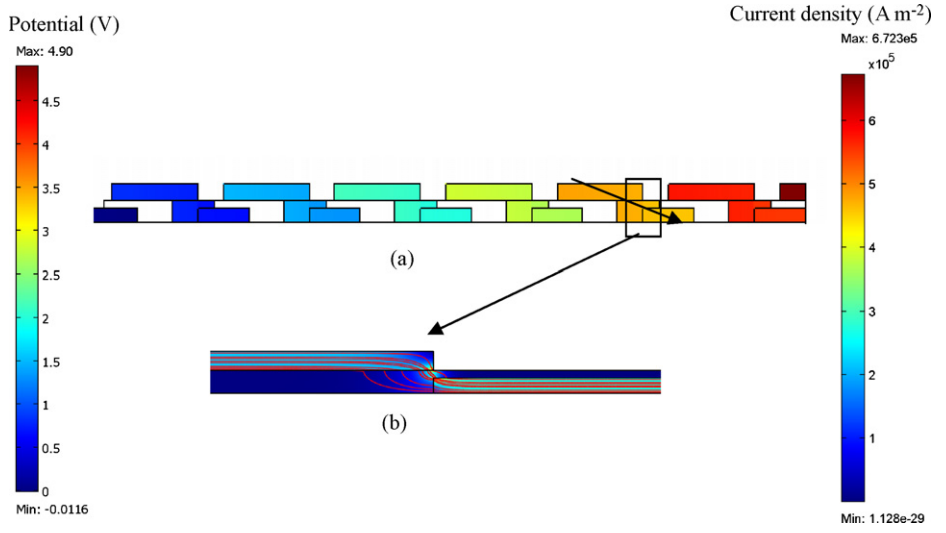

Fig. 3. (a) Potential (V) distribution of the SS-SOFC. (b) Streamline and distribution plots of current density (A m^{-2}) from the cathode via the interconnector to anode.

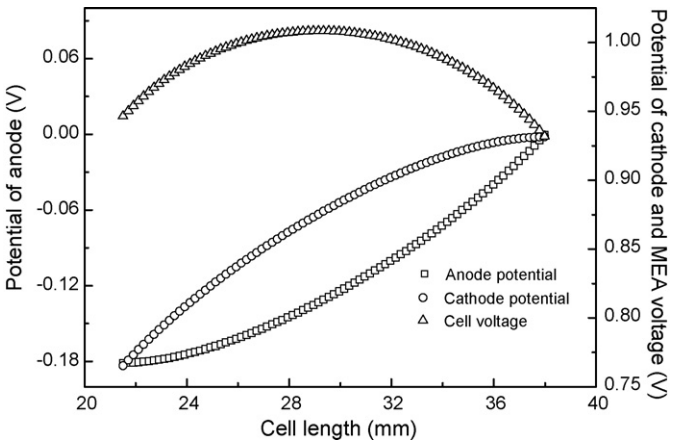

Fig. 5. The voltage (V) of the second MEA, the potentials of its cathode and anode for 18 mm anode length with support substrate of 0.8 mm inner radius and the cathode of 50 μm thickness.

in the gas channel and the electrodes:

$$\nabla(-D_{ij} \cdot \nabla c_i + c_i \cdot u) = 0 \tag{4}$$

Anode/electrolyte interface boundary:

$$(-D_{H_2,a} \nabla c_{H_2} + c_{H_2} u) \cdot n = -\frac{i_a}{2F} \tag{4a}$$

$$(-D_{H_2,a} \nabla c_{H_2O} + c_{H_2O} u) \cdot n = \frac{i_a}{2F} \tag{4b}$$

Anode channel inlet:

$$c_{H_2} = c_{H_2,0} \tag{4c}$$

$$c_{H_2O} = c_{H_2O,0} \tag{4d}$$

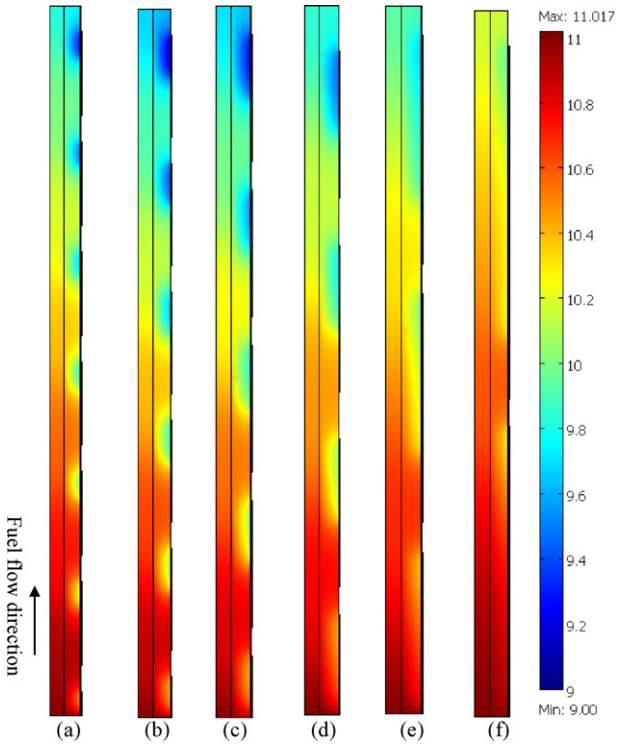

Fig. 6. Surface plots of H_2 concentration (mol m^{-3}) distribution for the different anode length of the SS-SOFC (anodic length from (a) to (f) is 3, 4, 5, 7, 10 and 18 mm, respectively).

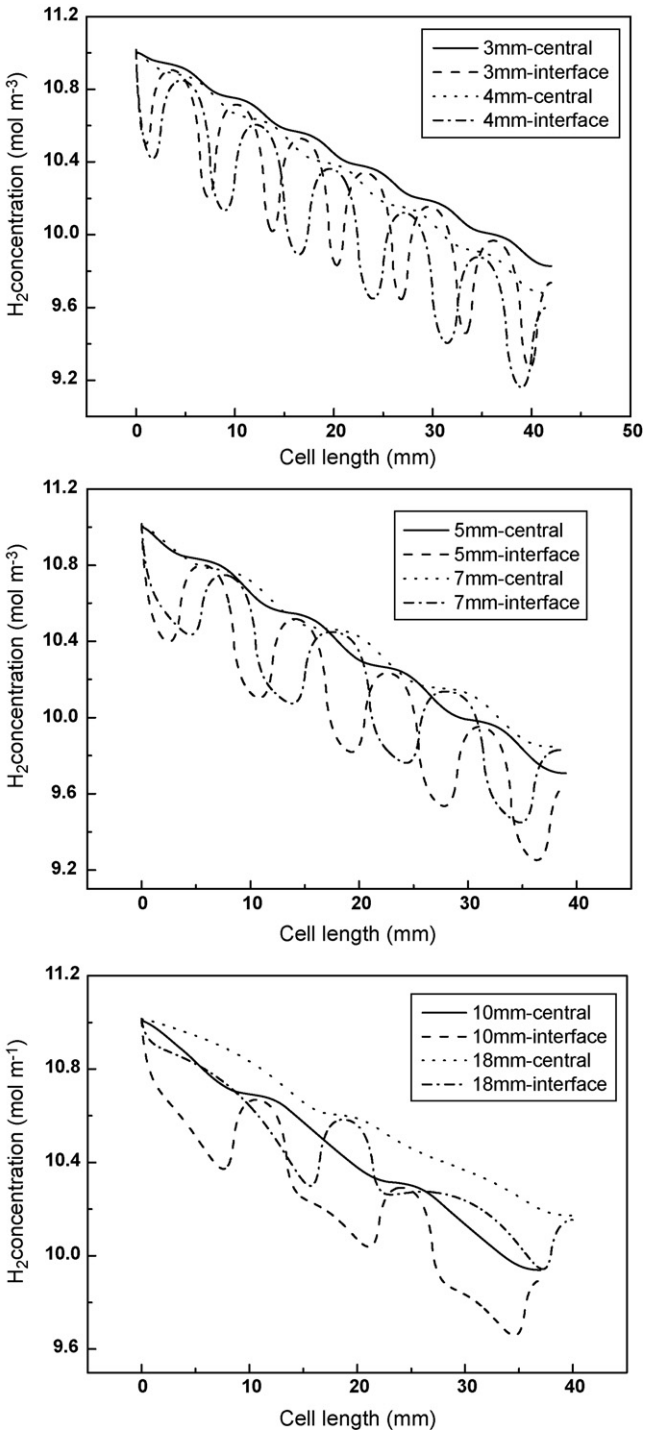

Fig. 7. H_2 concentrations (mol m^{-3}) along the anode/substrate interface and fuel channel center in the SS-SOFC of the different anode lengths.

Cathode/electrolyte interface boundary:

$$(-D_{O_2,c} \nabla c_{O_2} + c_{O_2} u) \cdot n = -\frac{i_c}{4F} \tag{4e}$$

O_2 concentration at cathode/air interface:

$$c_{O_2} = c_{O_2,0} \tag{4f}$$

The governing equations are solved with the commercial software, COMSOL MULTIPHSICS. In this article, we choose to create a free mesh consisting of triangular elements for a 2D geometry in COMSOL Multiphysics. In these calculations, mesh consists of about

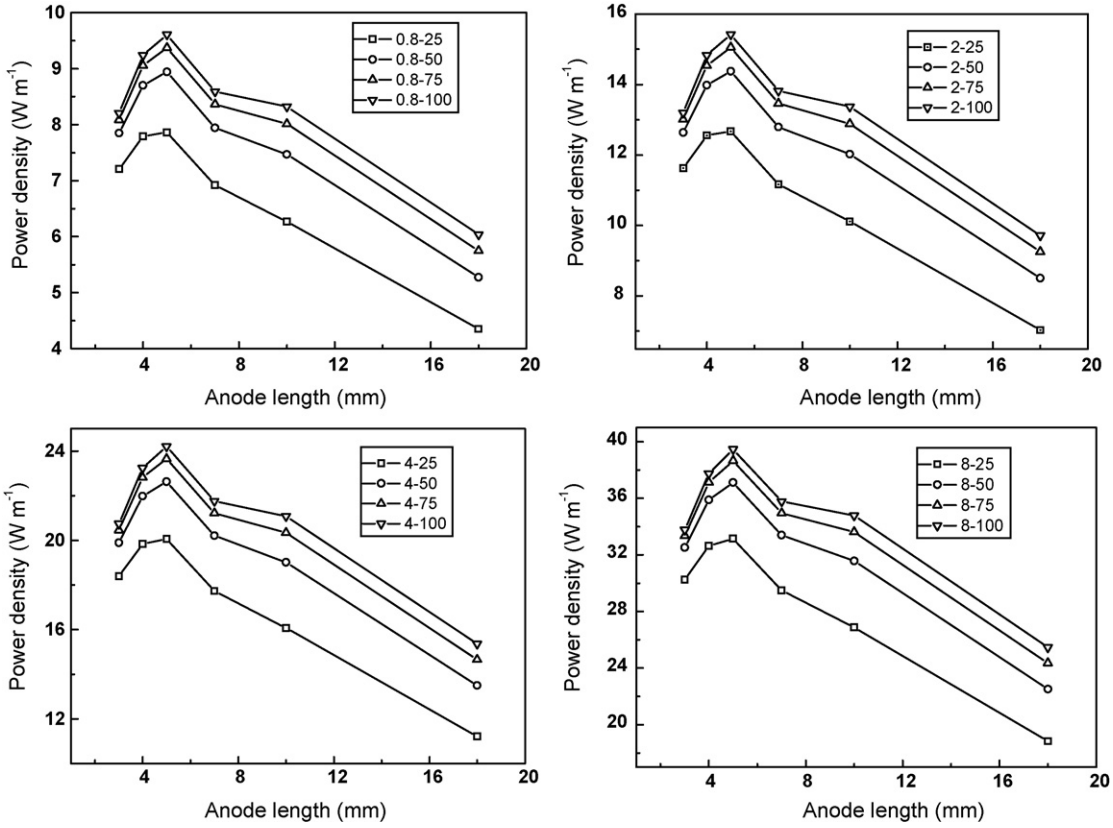

Fig. 8. Effects of different geometries on power density of the SS-SOFC.

140,000 elements. The convergence criterion is relative tolerance of 1e−6.

3. Results and discussion

3.1. Transport phenomena analysis in SS-SOFC

The potential distribution of the cell module is shown in Fig. 3. The potential is highest on the right-hand side where the cathode connects with the current collector. The lowest potential is on the left-hand side where the anode connects with the current collector. As far as the cell module is concerned, the potential deceases from right to left. For the change of the local potential in Fig. 3, it is shown that the potential deceases from left to right inside the rectangle and the arrow shows the current direction. At the connecting region of two unit cells, the potential decease from the cathode via the interconnector to anode.

The distribution of the current density is not uniform in the unit cell. To comprehend the flow of the current in the SS-SOFC, the streamline and distribution plots of current density ($A\,m^{-2}$) from the cathode via the interconnector to anode are shown in Fig. 3. The part enclosed by the rectangle in Fig. 3(a) is scaled up to Fig. 3(b). The streamlines express current-flow directions and paths. The current from the cathode to anode flows through interconnector with the shortest path, which is because the electrical conductivity of the interconnector is far lower than those of the electrodes. It can be seen that the highest current density occurs at this place where the path of the current is shortest from the cathode to the anode. The current flowing from cathode to anode is mainly via this area. The phenomena show that the most current-flow from cathode to anode crosses the interconnector from a very small area.

Fig. 4 shows the voltage of each membrane electrode assembly (MEA) with the support substrate of 0.8 mm inner radius and the cathode of 50 μm thickness. The anode length is changed as 3, 4, 5, 7, 10 and 18 mm. The voltage of each MEA is the potential difference between the cathode and the anode. The voltage of each MEA is higher than 0.7 V because of the ohmic loss from interconnector. Fig. 4 depicts that the voltage of each MEA decreases from fuel inlet to outlet because the fuel concentration decreases. The current flowing through each MEA in the SS-SOFC is same. However, the voltage is different at each MEA because the Nernst voltage of each unit cell is different. When the longer SS-SOFC is designed, the voltage is much lower at the last MEA than the front MEA. The anode of the last unit cell is at the relatively high oxygen pressure.

Fig. 4 also depicts that the voltage of each MEA exhibits a parabola-like curve. To understand this phenomenon, the voltage of the second MEA with the anode of 18 mm length in Fig. 4 is chosen. The chosen voltage curve is enclosed with the black half circle in Fig. 4. The potentials of its cathode and anode are also showed in Fig. 5. It indicates that the potentials of both cathode and anode increase from fuel inlet to outlet and express a protruding and concave curve, respectively. The voltage of each MEA is the potential difference between cathode and anode, so the voltage curve of each MEA is parabola.

The distributions of hydrogen concentration for the SS-SOFC of the different anodic length are shown in Fig. 6. Since the consumption of hydrogen occurs at the anode/electrolyte interface, the hydrogen concentration decreases along the fuel-flow direction. Fig. 6 shows that hydrogen concentration is low close to each anode. Fig. 7 shows the variation of H_2 concentrations ($mol\,m^{-3}$) along both the anode/substrate interface and fuel channel center of the SS-SOFC for the different anode lengths. The legend "3 mm-central" means the variation of H_2 concentrations along fuel channel center of the SS-SOFC for the anode length of 3 mm. The legend "4 mm-interface" means the variation of H_2 concentrations along the anode/substrate interface of the SS-SOFC for the

anode length of 4 mm. The H_2 concentrations of all cell modules are the same at inlet and decreases along the fuel-flow direction. The local H_2 concentration at the anode/electrolyte interface, where H_2 is consumed, is locally minimum. The H_2 concentrations show a sawtooth-like behavior, with the period set primarily by the anode length. A less-frequency oscillation can be seen when the anode length increases. The variation of H_2 concentrations along fuel channel center is similar to the H_2 concentrations at the active interface, but its variation is quite weak. Comparing Fig. 4 with Fig. 7, it is clearly seen that the variation of the local H_2 concentration causes the decrease of the voltage of each MEA from fuel inlet to outlet.

3.2. Improvement of cell geometry

The mathematical model is used to carry out the improvement of cell geometry. The effects of cell geometry on the cell performance are considered for the improvement of the SS-SOFC. The operating temperatures of all cells are 800 °C in the calculations. Fig. 8 displays the effects of the anode lengths on the power densities of the SS-SOFC. In this figure, power densities are calculated using power divided by the length of the cell module. The power densities decrease at longer unit cell lengths due to high resistance loss, whereas they decrease at shorter unit cell lengths due to less unit cell active area. The maximal power density is a result of the influences of both electrode resistance and unit cell active area with the change of the anode length. The optimal length of the anode is 5 mm, namely, the active length of unit cell is 3.5 mm.

Besides the anode length, the other key factors affecting cell performance are the cathodic thickness and the inner radius of the fuel channel. Fig. 8 shows the effects of both the cathode thickness and the inner radius of the fuel channel on the power densities for the different anodic lengths. An increase of the cathode thickness leads to a reduction of ohmic losses of the SS-SOFC, and causes a significant increase of the cell performance. The increment of power density is very little when the cathode thickness is larger than 75 μm, because the losses of the concentration diffusion play an important role for such a thick cathode. An increase of the inner radius of fuel channel can lead to an increase of cell module active area in the SS-SOFC, and thus raise the power densities.

4. Conclusions

The 2D mathematical models were developed to predict the electrical and species transport behavior in the SS-SOFCs of different geometries. The results indicate that the voltage of each MEA exhibits a parabola-like curve and is higher than the averaged voltage of unit cell (0.7 V). The voltage of each MEA deceases in the fuel-flow direction due to the decrease of the local H_2 concentration. When the electrolyte and interconnector gaps are fixed, the cell module with the anode length of 5 mm gives the maximum of power density for the SS-SOFC. Higher power densities can be obtained through increasing the cathode thickness. These calculations can be used to design and optimize SS-SOFC for the given materials and operating condition.

Acknowledgements

The authors gratefully acknowledge financial supports from the Ministry of Science and Technology of China (Nos. 2004CB719506, 2005CB221404 and 2006AA05Z147) and Natural Science Foundation of China (Nos. 20676132 and 20876156).

References

[1] S.C. Singhal, K. Kendall, High Temperature Solid Oxide Fuel Cells: Fundamentals Design and Applications, Elsevier, Kidlington Oxford, 2003.
[2] D.A. Cui, L. Liu, Y.L. Dong, M.J. Cheng, J. Power Sources 174 (2007) 246–254.
[3] D.A. Cui, M.J. Cheng, AIChE J. 55 (2009) 771–782.
[4] T.S. Lai, S.A. Barnett, J. Power Sources 147 (2005) 85–94.
[5] L. Repetto, P. Costamagna, J. Appl. Electrochem. 38 (2008) 1005–1010.
[6] P. Costamagna, A. Selimovic, M.D. Borghi, G. Agnew, Chem. Eng. J. 102 (2004) 61–69.
[7] L. Magistri, A. Traverso, F. Cerutti, M. Bozzolo, P. Costamagna, A.F. Massardo, Fuel Cells 5 (2005) 80–96.
[8] M. Cannarozzo, S. Grosso, G. Agnew, A.D. Borghi, P. Costamagna, J. Fuel Cell Sci. Technol. 4 (2007) 99–106.
[9] L. Repetto, G. Agnew, A.D. Borghi, F.D. Benedetto, P. Costamagna, J. Fuel Cell Sci. Technol. 4 (2007) 413–417.
[10] M. Loredana, B. Michele, T. Olivier, A. Gerry, F.M. Aristide, J. Eng. Gas Turbines Power-Trans. ASME 129 (2007) 792–797.
[11] S. Campanari, P. Iora, J. Power Sources 132 (2004) 113–126.
[12] P. Costamagna, K. Honegger, J. Electrochem. Soc. 145 (1998) 3995–4007.